NASA TECHNICAL MEMORANDUM

NASA TM X-71643

NASA TM X-71643

HEAVY ION BEAM PROBE MEASUREMENTS OF RADIAL POTENTIAL PROFILES IN THE MODIFIED PENNING DISCHARGE

by George X. Kambic
Lewis Research Center
Cleveland, Ohio 44135

TECHNICAL PAPER presented at
Sixteenth Annual Meeting of the Plasma Physics
Division of the American Physical Society
Albuquerque, New Mexico, October 28-31, 1974

HEAVY ION BEAM PROBE MEASUREMENTS OF RADIAL POTENTIAL PROFILES IN THE MODIFIED PENNING DISCHARGE

George X. Kambic*

Lewis Research Center

E-8203

ABSTRACT

A heavy ion beam probe is used to examine the radial potential profile of a plasma in the Modified Penning Discharge [1]. The plasma has strong ($\approx$ kV) electrostatic potentials near the anode ring which can be a large fraction of the injected ion beam energy. A primary (singly ionized) thallium ion beam is injected through the plasma in the midplane of a double Penning anode ring. After passage through the plasma, primary and secondary (doubly ionized) ions are detected with either a set of flat probes or an electrostatic energy analyzer. A calculation of the primary orbit through the plasma is performed to obtain an approximation to the measured primary beam trajectory. As the real radial potential profile is unknown, an adjustable model is used in the computer program. The adjustable potential profile is varied until the best agreement between measured and calculated trajectories is obtained. Secondary orbits are also predicted using the best-fitting adjustable profile. The calculations indicate that secondary beams originating at more than one point in the plasma can be simultaneously observed at the electrostatic analyzer with certain primary beam initial conditions. Such multiple secondary beams are observed near the predicted conditions.

INTRODUCTION

The heavy ion beam probe is a unique diagnostic for measuring spatially resolved space potential of a plasma. Previous use of the ion beam probe has been in devices where the plasma potentials, φ_s have been much less than the

*NASA-NRC Postdoctoral Associate.

primary ion energy, E_i/e, less than 10^{-2} E_i/e [2 and 3]. This report presents measurements using the primary beam of an ion beam probe in a plasma discharge where the space potential is a large fraction, $\gtrsim 0.1$, of the primary beam energy.

The Lewis ion beam probe is similar to that used by Jobes and Hickok in earlier work [3, 7-10]. A short explanation of the overall principle is presented here. A monoenergetic thallium (Tl) ion beam is injected into a plasma and part of the beam undergoes ionization to the Tl^{+2} state, with the dominant process being electron collisional ionization [2]. In this case, there is no significant change in the primary particle momentum. The magnetic and electric fields in the plasma volume cause the Tl^{+1} and Tl^{+2} beams to be separated. The primary and secondary beam energies can be measured in an electrostatic energy analyzer [9]. The primary beam current is also measured on any one of the set of 33 flat probes that make up the primary detector.

The ion beam initial conditions: energy, injection angle, and position; are input to the ion beam trajectory computation program. The object of this calculation is the determination of a potential profile such that computed trajectory end points of the primary beam are in agreement with the experiment. This is achieved by using an adjustable radial potential model as input to the computer program. For an assumed potential, secondary orbit end points are also predicted by this program.

The program is a modified version of a program written initially at Princeton [9] and used later at Rensselaer Polytechnic Institute [2]. The program solves the equation of motion of a charged particle of charge q and mass m in electric field E and magnetic field B which is

$$m \frac{d\vec{v}}{dt} = q(\vec{E} + \vec{v} \times \vec{B}) \qquad (1)$$

For specified magnetic and electric fields, the program computes the trajectory for a specified distance. The program can also choose points along the primary orbits where ionizations occur and then compute orbits for the secondaries.

The major difficulty in using an ion beam probe in this device is due to the plasma potential variations being a significant fraction of the primary beam ion energy. The difficulty results because the ion trajectories are significantly different from those of the negligible electric field case.

If these primary beam trajectories are known, then secondary ionization points can be predicted and a map made of the plasma potential. A second procedure feasible on this system is Abel inversion of the time of flight or the total deflection of the primary. Either of the quantities can be Abel inverted to give the electrostatic potential when the potential is assumed symmetric. This procedure has limited usefulness in the Modified Penning Discharge. The measurements given here indicate that the potential is nonmonotonic and, hence, the potential can be determined by this method only outside of the maximum. Whipple [4] and Dracott [5] have pointed out this problem. Johansson [6] operating an ion probe parallel to a magnetic field discusses measurement of potentials with minima and maxima.

APPARATUS

The Modified Penning Discharge [1] with the ion beam probe is shown in Fig. 1. The vacuum tank contains the two superconducting mirror coils and a high voltage double anode ring. The tank is 91.5 cm in diameter and 183 cm in length. It is pumped by one 25 cm diffusion pump. Access is provided by six ports along the sides of the tank and two ports on the tank ends. All surfaces in the tank except the anode are grounded. The anode ring support shaft comes into the field through a midplane port on one side of the tank. Access for the electrostatic analyzer, which is at left center of Fig. 1, is through the second center port on the opposite side of the tank. Access for the ion gun is through a port installed on the magnetic midplane beneath the anode ring port. The superconducting mirror coils are capable of 2.0 Tesla in the mirror throat and in the present

mirror configuration used herein have a mirror ratio of 2.5:1. The coil throat is 16.5 cm in diameter and the mirror points are 36 cm apart.

Figure 2 shows a cutaway drawing of the plasma region. The magnet spacer bars in Fig. 2 support the loads between magnet coils. One of these bars can interfere with some measurements as described later in this report. The double anode ring is shown in the midplane of the mirror field. The anode ring is 0.64 cm diameter tubing, bent into a 15 cm diameter circle with the two loops 2.5 cm apart axially. It is water cooled during operation. The mesh screen, which is at ground potential, is 27 cm in diameter, surrounds the anode ring, and has an extension to cover the anode support shaft. The screen is perforated stainless steel except for a coarse mesh which is woven over those regions where the ion beam passes. The relative locations of the ion gun and the electrostatic analyzer are also shown. Both the ion gun and the electrostatic analyzer are in the midplane of the magnetic field.

Figure 3 shows the probe elements in a schematic cross section of the system. The locations of the ion gun and electrostatic analyzer are shown with respect to the anode ring. The ion gun is a two element, electrostatic focusing and accelerating system with a thermionic thallium zeolite source [9]. A pair of deflection plates is placed at the low voltage end of the gun and is used to vary the beam direction. The gun is maintained in a bell jar that is removable from the main tank while the main tank is still under vacuum. An optical baffle for the gun is positioned just inside the main tank wall. This shield is useful in eliminating electrical breakdown problems in the gun. The electrostatic analyzer entrance slit is positioned close (2.5 cm) to the horizontal plane of the system. The analyzer is designed for a mean entrance angle of 45°. Ions are deflected into the split plate detector [9]. The bell jar containing the electrostatic analyzer is differentially pumped. The flat probes are shown in the upper quadrant nearest the electrostatic analyzer. The primary detector is fixed in position. Each flat probe is 1 cm wide and 1 mm gaps separate adjacent probes. The primary detector covers a 42° angular region on the tank wall.

The typical midplane magnetic field is 0.46 Tesla with a throat field of 1.2 Tesla. The base pressure of the system with LN_2 and LHe temperature surfaces assisting in cryopumping is $\approx 6\times10^{-8}$ torr. The discharge is

run in deuterium gas pressure up to 10^{-4} torr. The power supply for the Modified Penning Discharge anode is capable of 40 kV DC at 1 amp. The discharge is capable of long-term steady-state operation.

Typical discharge operation for data reported herein is $V_{anode} \sim 10$ kV, $I_{anode} \sim 10$ ma, and pressure $\sim$ 13-16 μtorr. The ion gun is operated at voltages from 6 kV to 35 kV. The deflection plates are operated at voltages to deflect the beam $\pm 5^{o}$ around the gun centerline. The electrostatic analyzer is operated from 0 to 50 kV. A typical primary ion beam current is 0.5 μamp. The primary detector probes are grounded through 1 kΩ resistors to prevent charging.

The ion beam is adjusted to impinge on a given ion detector by directly measuring with a Tektronix Type 555 scope the primary beam (about 0.5 μamp) arriving on the detector as a function of ion beam injection angle. The injection angle is varied by applying a constant potential plus a 0-150 sawtooth output from the oscilloscope to the deflection plates. Beam impingement in the detector is confirmed by measuring the detector current with a PAR HR-8 lock-in amplifier. For constant injection angle operation, the detector currents are measured with a Keithley 310 DC ammeter.

EXPERIMENTAL PROCEDURE

In this study, the approximate radial potential profile is obtained by observing the effect of the plasma on the trajectory of the primary beam. There are two usable detectors; the electrostatic analyzer, and the primary detector made up of 33 flat probes positioned in the beam path on the tank wall.

In the procedure used here, the primary beam end points were first measured with the anode voltage off. These results are given in Table I, which lists the beam energy injection angle and end points for both measured and calculated cases. At $E_i \approx 6$ keV, the primary beam is observable in the electrostatic analyzer, while at higher energies it is observable on the primary detector. The location of the beam on the primary detector

is specified by (r, θ) coordinates. In Table I, the measured end point for the higher energy cases is the fourth detector above the analyzer at r = 42.7 cm and $\theta = 25.4^{o}$ in the tank coordinate system. The primary beam calculated paths are not in exact agreement with the measured locations. When the injection angle is set equal to that calculated from the voltage on the ion gun deflection plates, the beam is calculated to intercept the primary detector approximately $1\frac{1}{2}^{o}$ below the measured location. For the magnetic field strength used for results reported here, an energy of $E_i \approx 6$ keV was required to deflect the beam into the electrostatic analyzer.

Changing the thermionic source in the ion gun affected the location of the effective ion emission point. For example for two different sources, where $E_i \approx 6.1$ keV, two different deflection voltages were required to deflect the beam into the electrostatic analyzer. Also two different deflection voltages were needed to deflect the beam to the primary detector. The relative differences between the angles remained the same as shown in Table II.

In general, the beam end point, when the plasma is off, "rises" as a function of increasing energy. This means the defining angle between the x-axis and the beam final velocity increases. This is, of course, expected. An error in the ion emission point on the order of 2 cm could also explain the error in the calculations for no plasma. However, this error is less likely than that for the injection angle. As a result of these no plasma tests, it appears that the true beam injection angle may deviate from the apparent injection angle by as much as 2^{o}. For the initial measurements reported herein, this deviation was not considered to be sufficiently large to significantly alter the calculated potential distribution.

Table III lists primary beam trajectory results for various plasma discharge conditions. The primary beam energy, the injection angle calculated from the measured deflection voltage, the measured end point, and plasma conditions of anode voltage and pressure are given. The primary energies varied from 11.5 keV to 37 keV and the injection angles spanned

the mean angle of 39.3^{o} by $\pm 4^{o}$. The plasma voltage ranges from 4.5 kV to 17 kV and the tank pressure from 0.8 μtorr to 47 μtorr. However, the majority of points were taken at an anode voltage $V_a \sim 10$ kV and a tank pressure P ~ 13-16 μtorr. In all cases the primary beam was detected in either the electrostatic analyzer or one of the five primary detector plates closest to the analyzer. A spacer bar blocked access to about six plates above this. The primary beam was never on the detector plates above the spacer bar.

The data in Table III can be separated into a number of divisions. The first ten cases were listed in pairs. These were double sets obtainable under a single plasma condition. These sets would enable a simultaneous double check to be made of the adjusted model potential profile in the computer program. Below this are listed single data points of observations. In the range of parameters covered, there were only a few conditions in which a secondary beam signal could be detected with the electrostatic analyzer.

For the no plasma case, positive deflection angles were required to deflect the beam to the primary detector and there was only a single beam energy (~6 keV) and deflection angle case that would reach the electrostatic analyzer. For discharge operation at low anode voltage, (~5 kV) the beam ($E_i \sim 6$ keV) was no longer observable in the analyzer. At higher beam energies, the beam was observed on the primary detector at deflection angles ~39.3^{o}. Beam energies, E_i = 19.8 keV, 30.6 keV, are examples of this.

At anode voltages above 5 kV for the pressure regime 0.5 μtorr to 16 μtorr, this situation changed. At beam energies in the range 11.5 keV to 22.0 keV, the beam required a deflection $<39.3^{o}$ to be observed on the primary detector and a deflection angle $>39.3^{o}$ to be observed in the electrostatic analyzer. This result was both surprising and interesting because a plot of the orbital path at the energy and deflection angle of interest indicated that the magnetic effect on the beam path was overcome

by the effect of the electrostatic potential. Also, the beams which had injection angles $>39.3^{o}$ have to be deflected $\gtrsim 40^{o}$ in order to be observed in the electrostatic analyzer.

ANALYSIS OF RESULTS

The experimental results given in Table III were examined using an orbit computation program with an assumed potential profile. In order for this to be done, an initial estimate of the radial electrostatic potential profile is inserted into the program. The model parameters shown in Fig. 4 divide the radial potential profile into four regions. In two of these regions, the potential is constant. These regions are $0 \leq r \leq R_r$ and $R_i \leq r \leq R_o$. The potentials in these regions are specified in the model by φ_{in}, and φ_{max}, respectively. For $R_o \leq r \leq R_{ground}$, the potential is assumed to be a linear function of r, which is a good approximation to the vacuum field, as shown in Fig. 5. The vacuum field in Fig. 5 is obtained from a computer solution of Laplace's equation in cylindrical symmetry when the potentials are specified on the anode ring and grounded screen. The program is described in [12]. Inside of the radius R_i, the model potential is proportional to r^2 plus a constant, which gives an electric field proportional to r in this region, consistent with the results of [4].

To optimize the model parameters, we utilize a minimization procedure, using the quantity M, given in Eq. (2),

$$M = \sum_{i=1}^{n} (\theta_{mi} - \theta_{ci})^2 \qquad n = 1, 2, \ldots \tag{2}$$

where the angles in the above expression are the coordinates of the intersection point of the trajectory at the radius of the detector. θ_{mi} and θ_{ci} are obtained from the measured and calculated beams, respectively. In general, n initial beams can be injected into the same potential, however, $n = 2$ for the cases reported here. The calculated θ's are a function of

the five parameters (R_i, R_o, R_r, θ_{max}, θ_{in}) and, hence, so is M. The actual procedure of minimization involves a choice of an initial guess and the iterative variation of the five parameters. The order of variation was θ_{max}, R_r, θ_{in}, R_i, and R_o. The initial guess is shown in Fig. 5. This initial guess is consistent both with vacuum field solution for $r > R_o = R_{anode}$ and the discussion of [4] for $R_r \leq r \leq R_i = R_{anode}$. The primary beam initial conditions and trajectory end points are taken from Table II(a). The actual initial guess for both cases examined in detail is specified by $R_i = R_o = R_{anode}$, $R_r/R_{anode} \sim 0.87$, $\varphi_{in} = 0$ and $\varphi_{max} \sim 0.88\ V_{anode}$. This is shown in Fig. 5 along with the vacuum field.

The detailed iteration processes used are described in the appendix. The cases examined in detail were the first two pairs from Table II. The results of the minimization of M for these data is given in Fig. 6 as radial potential profiles. The characteristics of the profiles are also listed on this figure. The general characteristics of the potentials are: (1) φ_{max} is close ($\gtrsim 0.9\ V_{anode}$) to V_{anode}; (2) there are nonzero potentials on axis. The interesting result that $R_i > R_{anode}$ has two pieces of evidence in its favor: (1) the location of $R_i/R_{anode} > 1$ and $R_o/R_{anode} > R_i/R_{anode}$ minimizes M, and (2) this potential seems to describe multiple secondary ion orbits that are observed in the experiment and will be discussed later. It does not seem physically possible for this maximum to be shifted away from the location of the anode. Whether it can be attributed to the minimization process involves a more careful examination of errors that may arise in the measurement process.

Within experimental error then, the potentials in the Modified Penning Discharge are at a maximum close to the anode voltage, and nonzero on axis. Some fields exist through the whole plasma region. This result is consistent with electron beam probing results by Dow [13] of a Penning discharge. However, his device was much smaller (which may account for the shapes of the potentials). At low pressures ≈ 1.5 μtorr in his device there are nonzero potentials in the center, at $r = 0$. Dow indicates that as pressure is increased, the potential in the center decreases. This result may

correlate with the result on Fig. 6, since curve (1) was taken at a pressure of ≈16 μtorr while curve (2) was taken at ≈1.0 μtorr. Finally this nonzero potential on axis implies the existence of axial electric fields in this device which could be examined by a process similar to Johansson [6].

The process of minimization itself can continue to a final answer which is more numerically precise than we can achieve with measurement error in the experimental parameters, for example, the anode voltages are known no better then ±2 percent, so that there can be an error of a few hundred volts. In the minimization calculations, the sensitivity of M to small parameter changes indicates that our parameters can be determined accurately. However, unless the ion orbits cross the discharge center, we do not have direct knowledge of any region inside the distance of closest approach of the ion trajectory to the center. One method of eliminating this problem is the use of the secondary ion technique [10]. Direct use of the Hickok-Jobes technique using high energy beams would eliminate the ambiguities and give direct measurement of the plasma potentials. Primary beam energies required would be on the order of 200 keV. The technique of adjustable potentials, used here for the primary beam, is also possible. The profile can be adjusted until it correctly predicted all measured secondary energies.

Both profiles in Fig. 6 were used to predict possible secondary ion orbital paths from points along the ion beam. The result was that under some plasma conditions, for example, those in case 1 in Table III; multiple secondary orbits can originate in the plasma which reach the electrostatic analyzer entrance slit and have their energy measured. Figure 8 shows the results of a calculation of secondary orbits. The potential from case 1 of Fig. 6 was used in this calculation. The energy and orbit of the primary particle are specified. The calculation indicated that if the potential was that given in Fig. 6, then secondary ions emitted at three points in the plasma region would enter the electrostatic analyzer. The energies and emission points are specified in Table V and are also shown on Fig. 8. It is necessary to point out that these are calculated results. It is unusual in ion beam

probing to see more than one secondary beam from a single primary beam. However, in the experiment, multiple peaks were observed in the energy spectrum of the secondary beam at the beam and plasma conditions listed on Fig. 8. For comparison purposes, these peaks are listed in Table V and are also given in Fig. 8. It is not expected that the profiles used in computer calculations should provide all the correct energies of the measured secondaries. Further adjusted profiles would have to be used to find the correct solutions. The intention of Table IV and Fig. 8 is to indicate that we have approximated a possible correct solution. The primary beam is observed in the electrostatic analyzer as predicted by the computer. The difference between calculated and measured values of secondary ion energies ($\approx$10 percent) shows that slight additional adjustment of the model potential profile is required to minimize differences between both primary and secondary calculated and measured orbits.

CONCLUDING REMARKS

The Lewis Ion Beam Probe is working as a true ion beam probe. Using it first as a primary ion probe, we are able to obtain a satisfactory radial potential profile. Strong electric fields are indicated by the size of the potentials. Calculations based on one of the profiles indicate that the primary beam orbits can emit observable secondaries from more than one ionization point in the plasma. The multiple peaks provide confirmation of the model profile. Their prediction and observation provides a cross check of the model profile and lends credence to the modeling procedure. To use this technique in a plasma where the potentials approach the beam ion acceleration potential requires a model of the potential profile. The model can be tested by this technique to show whether or not it is valid.

APPENDIX - MINIMIZATION OF M

The iteration processes concentrated on obtaining solutions by minimizing the quantity M, given in Eq. (A1).

$$M = \sum_{i=1}^{n} (\theta_{mi} - \theta_{ci})^2 \qquad n = 1, 2, \ldots \tag{A1}$$

where the angles in M are the coordinates of the intersection point of the trajectory at the radius of the detector. $\theta_{m,c}$ refers to measured and calculated angles, respectively.

The computer program inputs for the potential profile were φ_{max}, φ_{in}, R_r, R_i, and R_o. φ_{max} was kept less than V_{anode} because the plasma cannot float higher in potential than the anode voltage. Also, the requirement on radius that $0 \leq R_r < R_i \leq R_o < 13.5$ cm was observed. φ_{max} was assumed greater than φ_{in}.

Typical values for the starting point of the calculation were $\theta_{in} = 0$, $\varphi_{max} = 0.88\, V_{anode}$, $R_r = 6.5$ cm, and $R_o = R_i = 7.6$ cm. The order of parameter variation was φ_{max}, R_r, φ_{in}, R_i, and R_o. R_i and R_o were initially set equal to one another and varied independently only after M was minimized with $R_i = R_o$ at some radius r. In the first iteration loop the parameters were varied in step sizes $\approx$10 percent of their maximum values. As the parameter ranges that minimized M were found, the step size of the changes was reduced, first to $\approx$5 percent. Around the final minima, changes in φ_{max} and φ_{in} were $\lesssim$1 percent, and for R_i, R_o, and R_r $\lesssim$2.5 percent. The sensitivity of M to the various parametric variations of the adjustable parameters about their final values is shown in Fig. A1. A1(a) is for case 1 and A1(b) is for case 2. M is quite sensitive to changes in the parameters. Hence, this increases our confidence in the results determined in this report.

ACKNOWLEDGEMENT

The author thanks Robert Hickok and Robert Reinovsky for their helpful discussions and computer program assistance.

REFERENCES

1. Roth, J. R.; Freeman, D. C., Jr.; and Haid, D. A.: Superconducting Magnet Facility for Plasma Physics Research. Rev. Sci. Inst., vol. 36, no. 10, Oct. 1965, pp. 1481-1485.
2. Reinovsky, R. E.: An Ion Beam Probe Diagnostic Technique for Laboratory Plasma. RPDL-73-13, Rensselaer Polytechnic Institute (AFOSR-TR-74-0242; AD-775051), 1973.
3. Hosea, J. C.; Jobes, F. C.; Hickok, R. L.; and Dellis, A. N.: Rotation and Structure of Low-Frequency Oscillations Inside the ST-Tokamak Plasma. Phys. Rev. Letts., vol. 30, no. 18, Apr. 1973, pp. 839-842.
4. Whipple, R. T. P.: On the Determination of Magnetic Fields in Slabs and Cylinders by Measurement of Time-of-Flight or Displacement of Monoenergetic Ions which are Projected away from the Wall and Returned by the Magnetic Field. AERE R-3486, Atomic Energy Research Establishment, 1960.
5. Dracott, E. D.: A Method of Measuring the Potential Distribution in a Cylindrical R.F. Cavity Containing Plasma. J. Electronics and Control, vol. 10, no. 1, Jan. 1961, pp. 25-32.
6. Johansson, R. B.: Electric Potential Measurements by Ion Beam Probing, TRITA-EPP-71-26, Royal Institute of Technology, 1972.
7. Jobes, F. C.; Marshall, J. F.; and Hickok, R. L.: Plasma Density Measurements by Ion Beam Probing. Phys. Rev. Letts., vol. 22, no. 20, May 1969, pp. 1042-1045.
8. Hickok, R. L.: Plasma Density Measurement by Molecular Ion Breakup. Rev. Sci. Inst., vol. 38, no. 1, Jan. 1967, pp. 142-143.
9. Hickok, R. L.; Jobes, F. C.; Marshall, J. F.: Beam Probe Mapping of Rapidly Fluctuating Plasma Density in an Energetic Arc. Mobil Research and Development Corp. (AFOSR-69-0644TR; AD-687181), 1969.

10. Hickok, R. L.; and Jobes, F. C.: Heavy-Ion Beam-Probe Systems for Plasma Diagnostics. Mobil Research and Development Corp. (AFOSR-70-2354TR; AD-713857), 1970.
11. Roth, J. R.: Hot Ion Production in a Modified Penning Discharge. IEEE Trans. Plasma Science, vol. PS-1, no. 1, Mar. 1973, pp. 34-35.
12. Bogart, C. D.; Richley, E. A.: A Space Charge Flow Computer Program. NASA TN D-3394, 1966.
13. Dow, D. G.: Electron-Beam Probing of a Penning Discharge. J. Appl. Phys., vol. 34, no. 8, Aug. 1963, pp. 2395-2400.

TABLE I. - TYPICAL MEASURED AND CALCULATED PRIMARY ION BEAM TRAJECTORIES WITH DISCHARGE TURNED OFF

Primary beam		End point (r, θ)		Type result measured (M) or calculated (c)
Energy, keV	Injection angle, deg	cm	deg	
6.15	39.8	92.5	1.6	M
6.1	39.5		.8	C
6.1	40		1.0	C
6.2	39.5		1.1	C
6.2	40		1.3	C
20	41	42.7	25.4	M
20	41		26.6	C
22	42.2		25.4	M
22	42		24.5	C
22	42.5		24.6	C
17.8	42.5		25.4	M
17.8	42.5		22.2	C
31.8	39.5		22.4	M
31.8	39.5		20.3	C
18	43.1		25.4	M
18	43.1		22.4	C

TABLE II. - CHANGE IN ION BEAM TRAJECTORY

DUE TO CHANGE IN SOURCE LOCATION

Source	Beam energy, keV	Deflection voltage, volts	Injection angle, deg	(1 minus 2) deg
1	6.1	0	39.3	1.3
2	6.1	-40	38	
1	20	340	42.5	1.4
2	20	194	41.1	

TABLE III. - EXPERIMENTAL PRIMARY BEAM INITIAL CONDITIONS AND END POINTS FOR VARIOUS PLASMA OPERATING CONDITIONS

Primary beam		End point, r, $\theta \pm 0.5^{o}$		Plasma	
Energy, keV	Injection angle, deg	cm	deg	V_{anode}, kV	Pressure, μtorr
17.8	36.9	42.7	22.4	10.4	15.9
17.8	43.1	92.5	1.6	10.4	15.9
22.0	38.5	42.7	25.4	13.2	.8
22.0	42.9	42.5	1.6	13.2	.8
17.6	36.9	42.7	22.4	10	15.9
17.6	43	92.5	1.6	10	15.9
17.3	38.3	42.7	22.4	10.1	.5
17.3	43.1	92.5	1.6	10.1	.5
11.5	36	42.7	22.4	6	15.9
11.5	42.6	92.5	1.6	6	15.9
31.7	39.3	42.7	22.4	10	15.9
18	37.7	42.7	25.4	9.4	13.25
24.5	36.9	42.7	25.4	13.2	.8
23.6	42.9	92.5	1.6	17	13.25
23.1	37.6	42.7	20.9	7.5	↓
12.5	34.7	42.7	25.4	5.8	↓
16	47.86	92.5	1.6	12	↓
18	35.4	42.7	20.9	10	↓
18	35.2	42.7	22.4	10	↓
19.4	41.7	92.5	1.6	9.8	↓
19.8	44.3	42.7	22.4	4.5	↓
19.1	36.8	42.7	22.4	10	13.5
20.3	41	92.5	1.6	11.2	13.25
20.3	36.7	42.7	25.4	11.2	↓
30	38.6	↓	20.9	11.2	↓
30.6	42.7	↓	25.4	5.3	↓
37.2	38.9	↓	22.4	5.4	2.65
31.6	41.1	↓	26.8	5	53

TABLE IV. - COMPARISON OF CALCULATED AND MEASURED END POINTS FOR TWO DISCHARGE CONDITIONS

Primary beam		End point (r, θ) cm, deg			V_{anode}, kV	Pressure, μtorr
Energy, keV	Injection angle, deg					
(1) 17.8	36.9	42.7	22.4	M*	10.4	15.9
		42.7	22.2	C**		
	43.1	92.5	1.6	M	10.4	15.9
		92.5	8.9	C		
(2) 22.0	38.5	42.7	25.4	M	13.2	.8
		42.7	25.1	C		
	42.9	92.5	1.6	M	13.2	.8
		92.5	3.9	C		

*M (measured).
**C (calculated).

TABLE V. - CALCULATED SECONDARY BEAM TRAJECTORIES AND ENERGIES FROM CASE 1, TABLE IV AND COMPARISON WITH EXPERIMENT

Secondary beam		
Calculated energies		Measured energies, keV
Energy, keV	Ionization point (x, y) cm	
25	-9.2, -6.0	23
27	-8.2, -5.0	26.5
22	5.2, 3.0	19.8

E-8203

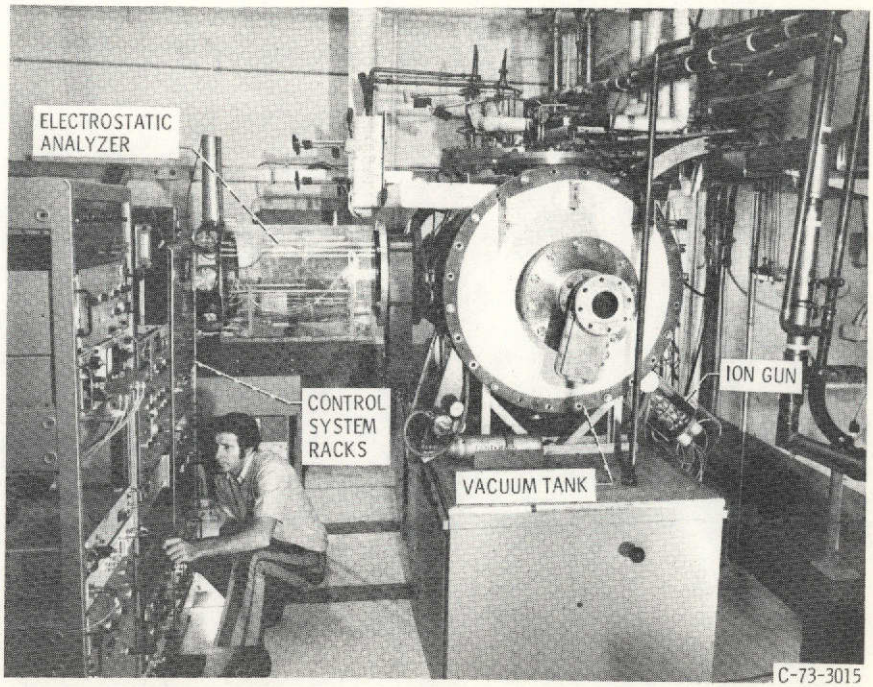

Figure 1. - NASA Lewis modified Penning discharge and ion beam probe facility.

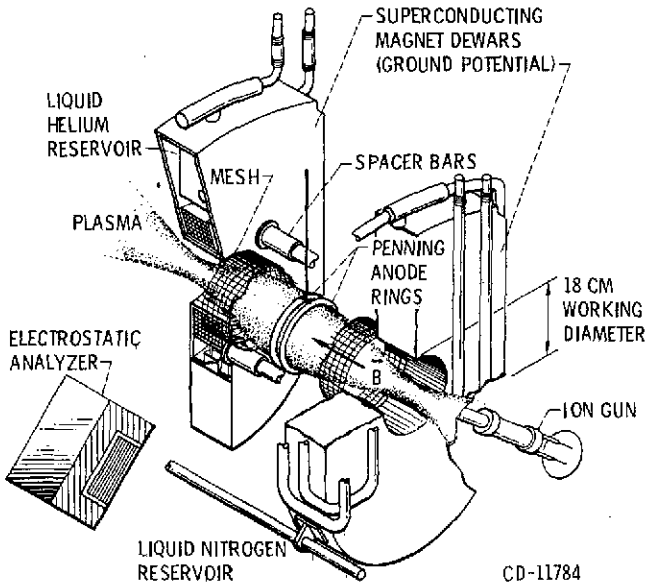

Figure 2. - Cutaway drawing of apparatus.

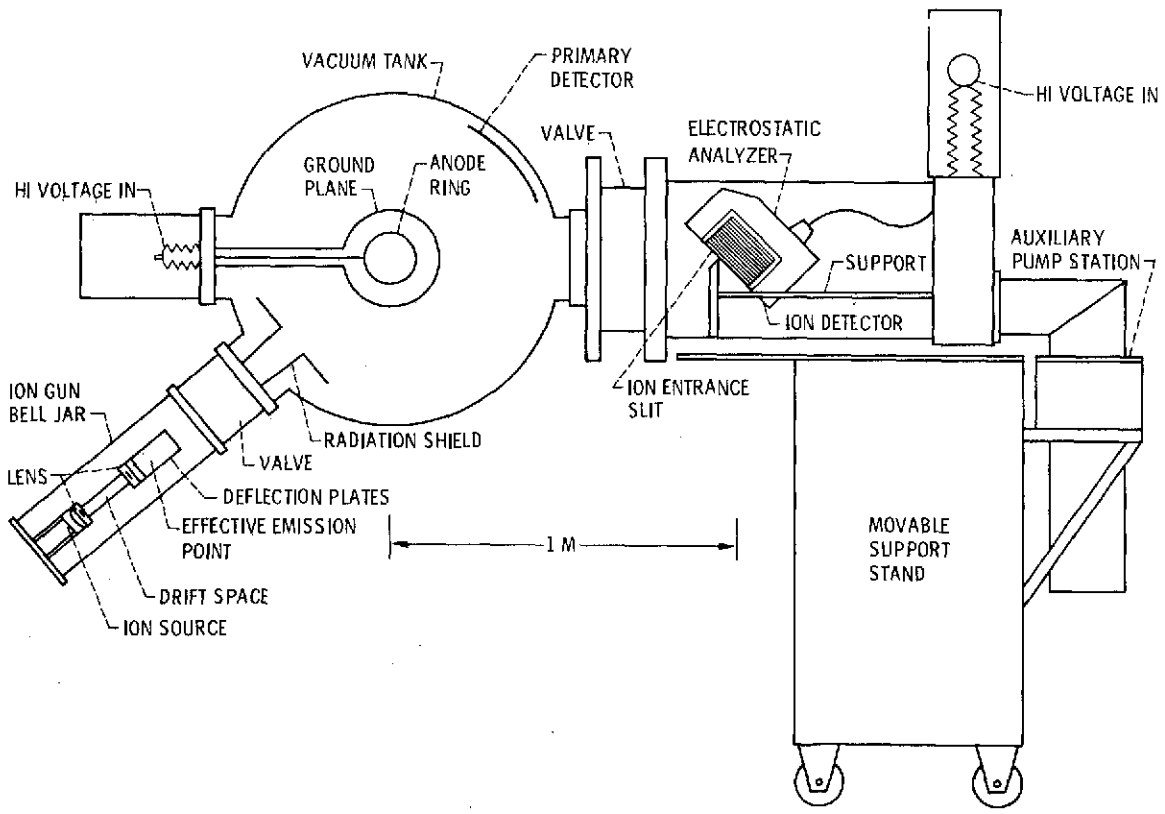

Figure 3. - Schematic of ion beam probe system.

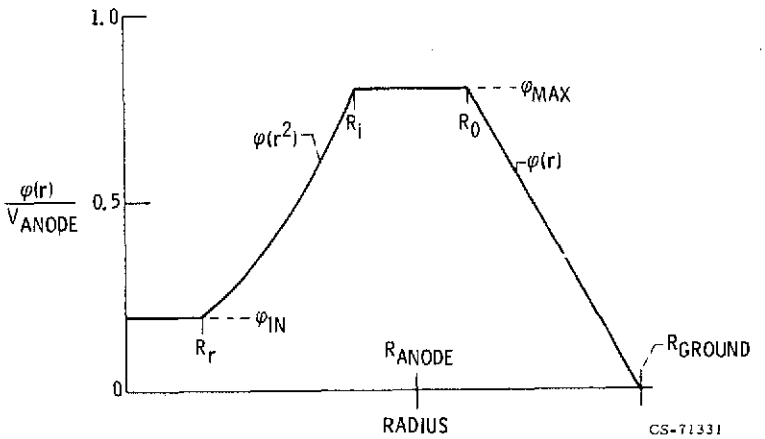

Figure 4. - Assumed model potential profile.

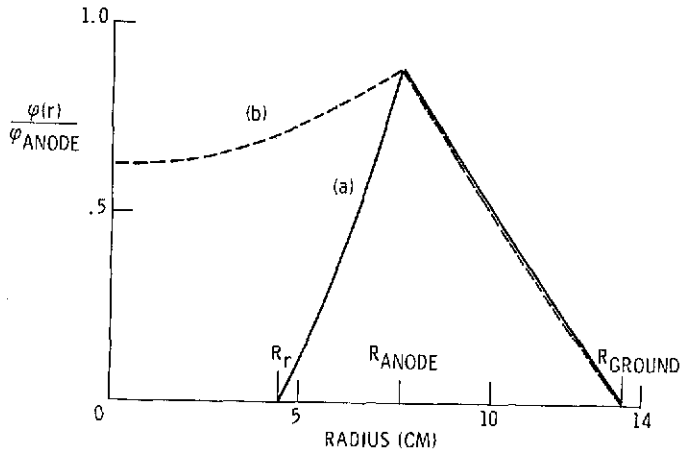

Figure 5. - Initial potential profile parameters (a) and vacuum field (b).

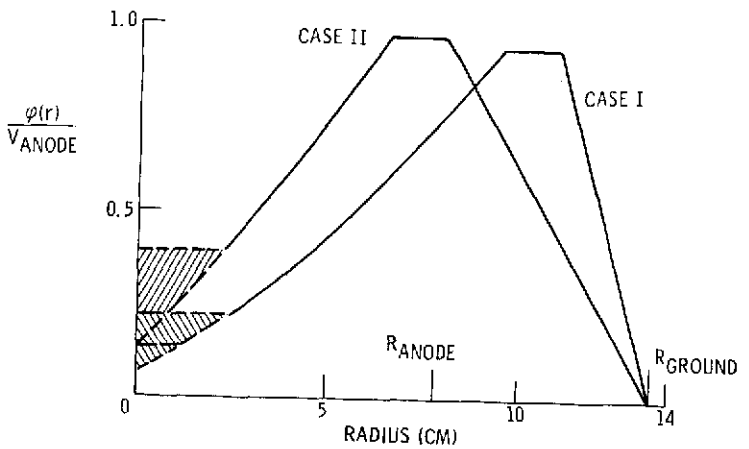

Figure 6. - Potential profiles for Case I and Case II, Table IV obtained by minimization of M.

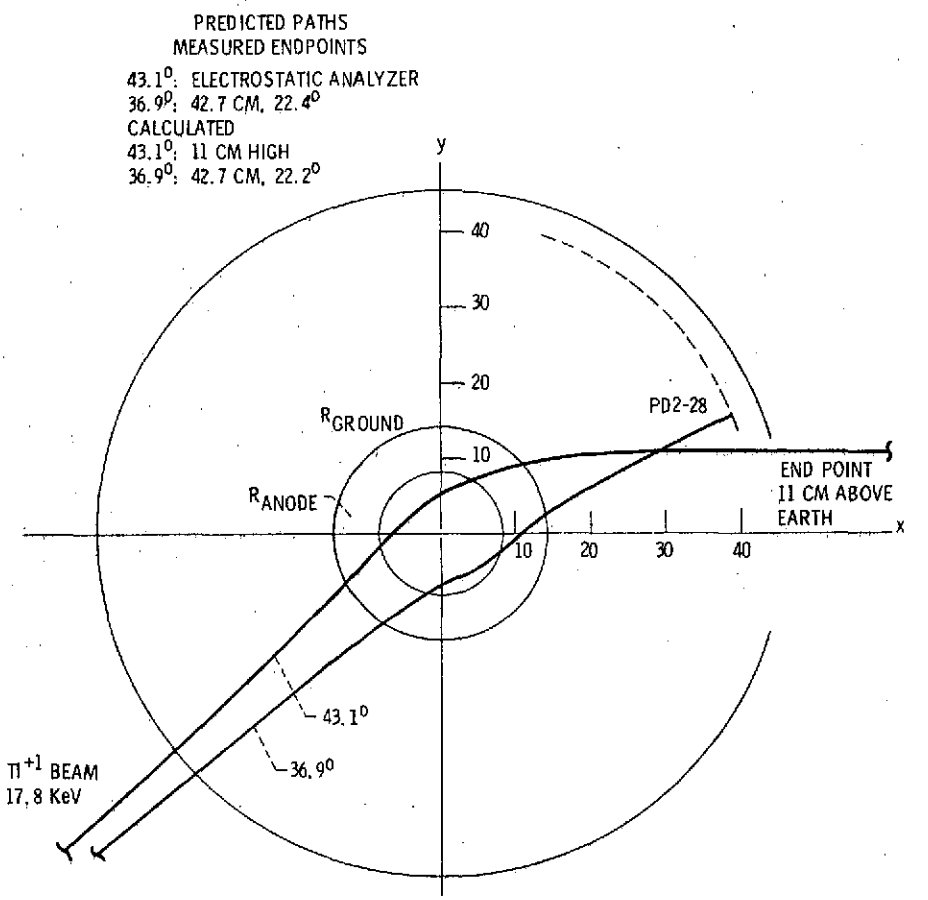

Figure 7a. - Calculated trajectories for model potentials (a) Case I, and (b) Case II.

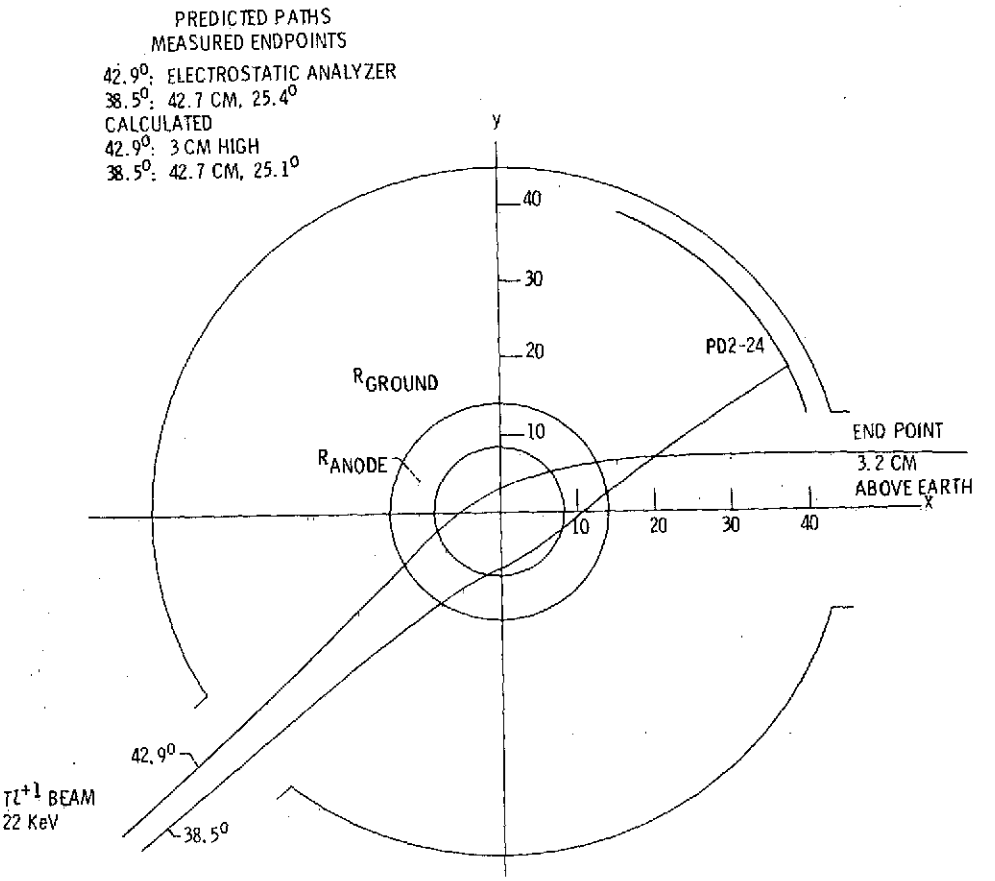

Figure 7b. - Case II.

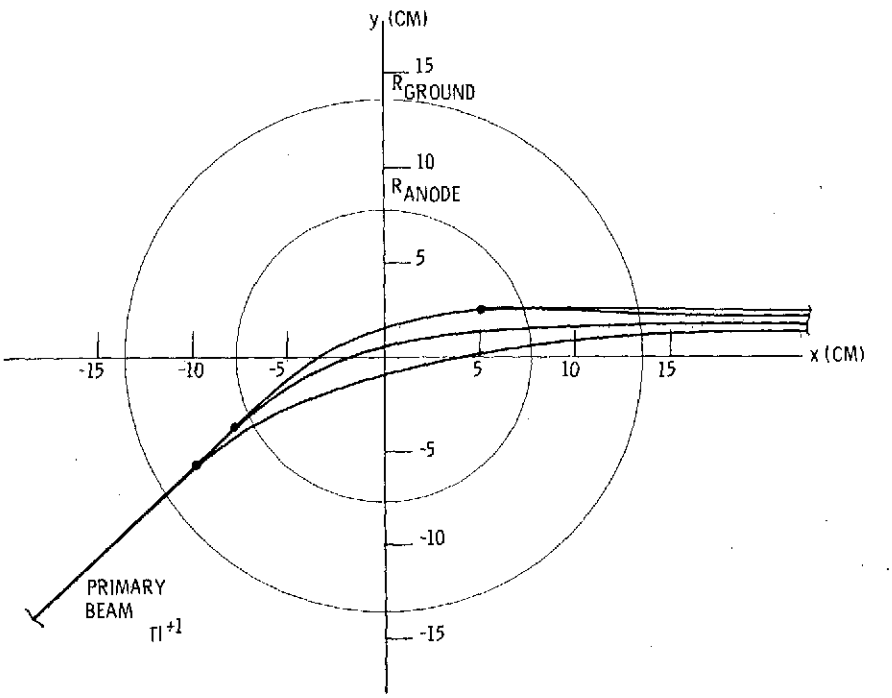

Figure 8. - Predicted secondary beam paths for Case I.

E-8203

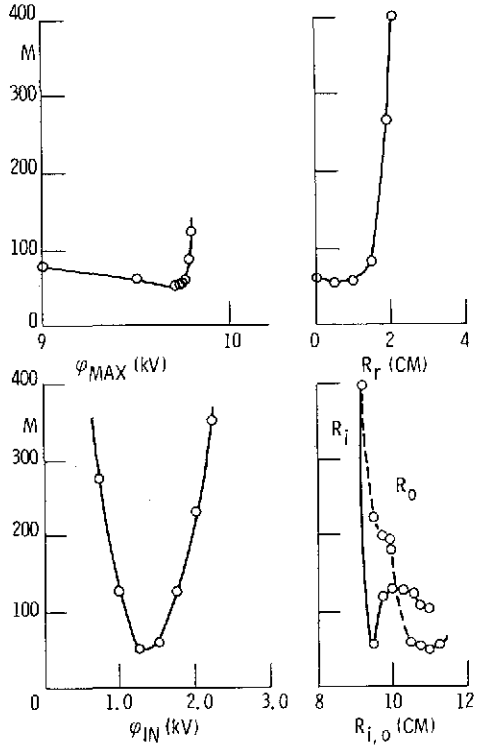

Figure A1(a). - Minimization of M as a function of model parameters for Case I.

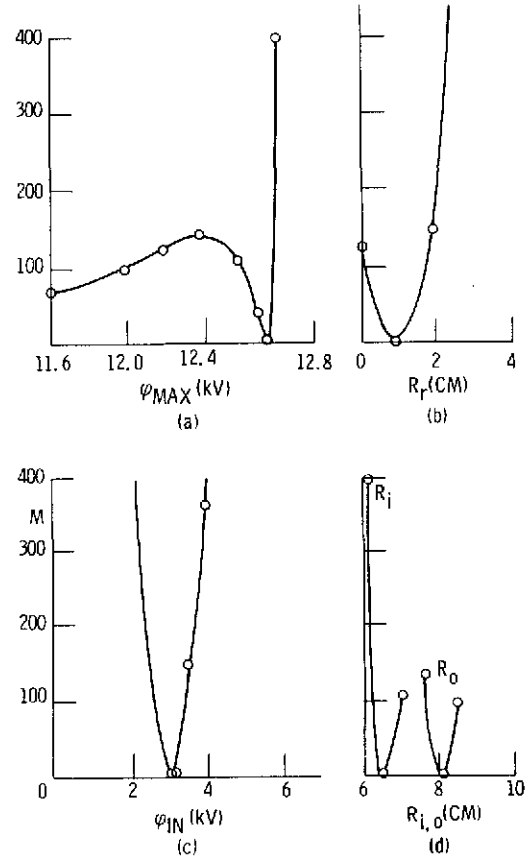

Figure A1(b). - M as a function of model potential parameters for Case II.